Pore Network Simulation of Imbibition into Paper during Coating: I. Model Development

Jaleh Ghassemzadeh and Mehrdad Hashemi
Dept. of Chemical Engineering, University of Southern California, Los Angeles, CA 90089

Luigi Sartor
Avery Dennison Corp., Avery Dennison Research Center, Pasadena, CA 91107

Muhammad Sahimi
Dept. of Chemical Engineering, University of Southern California, Los Angeles, CA 90089

A novel imbibition model of a coating fluid in a paper was developed. The microstructure of the paper was represented by a network of interconnected channels or throats formed between the paper's fibers. Geometrical characteristics of the channels, such as effective radius and length, were selected from representative statistical distributions. The interconnectivity of the channels was characterized by an average coordination number treated as a parameter of the model, and its effect on the imbibition process was studied. The study dealt with a dynamic (time-dependent) boundary condition, in which a convection-driven pressure was applied to the coating fluid on the external surface of the paper or driven only by capillary forces. The flow parameters used in the model represent a high-speed coating process. Extensive computer simulations were carried out to study the effect on the imbibition process of three distinct sets of parameters: microstructural parameters of the paper; the fluid's properties; and the dynamic boundary condition. The mean coordination number and average throat size of the paper's pore space, the coating fluid's viscosity, and the dynamic boundary condition all strongly influenced imbibition of the coating fluid.

Introduction

In many industrial processes it is often necessary to coat a porous substrate with a thin film of coating material in order for the substrate to have certain properties. The coating liquid is often deposited via one of the well-known high-speed coating technologies, such as die coating, roll coating, blade coating or any of several other methods. A prime example, which is the focus of our work, is paper which is often coated with a primer for improved printability or anchorage of subsequent coatings, or with a low surface energy material for use as a release liner in, for instance, a pressure sensitive adhesive construction, or label.

In the paper and label industry, coating is a widely-used process, both in paper making and the end products. The coating enhances the appearance and printability of the paper, and also gives it the required quality for further applications. It consists of applying a thin layer of mineral or organic emulsions or suspensions (hereafter referred to as the coating fluid) on the basepaper, followed by drying and calendering which are the finishing processes. The coating fluid consists typically of water, pigments, adhesive and processing aids. In this process the coating fluid is brought into contact in, for example, a slot coater with the paper which is moving at a constant speed (often called the web). The paper is composed of fibrous materials with fibers of a wide variety of thicknesses, lengths, and shapes, giving rise to a complex structure which in effect is a porous medium. The contact angle between the coating fluid and the paper's surface is usually low, so that it is regarded as a wetting fluid. The fluid coats the paper's external surface and also penetrates its pore structure. Since the coating liquid is a wetting fluid, its flow into the paper is an imbibition process, that is, penetration of

Correspondence concerning this article should be addressed to M. Sahimi.

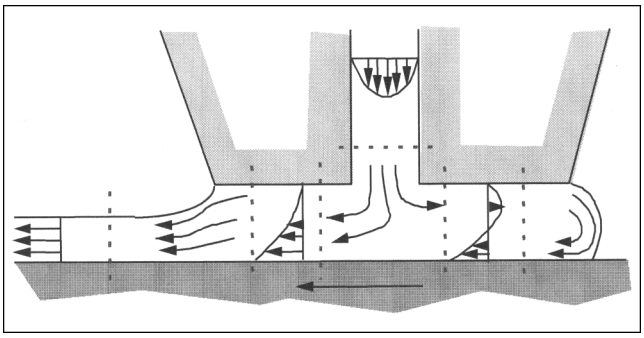

Figure 1. Coating system.

a wetting fluid into a porous medium saturated by a nonwetting fluid (Sahimi, 1993, 1995), which in this case is just air.

In the slot coating area, the coating fluid is distributed on the top surface of the paper and pushed into its pore space by an applied, convection-driven, pressure field, and hence flow of the liquid into the paper's pore structure is a forced imbibition process, whereas outside the slot coater the imbibition process is driven only by capillary forces, and thus in this area one has free or spontaneous imbibition. Figure 1 presents the system and the process, while Figure 2 shows the pressure distribution at the paper's top surface, both inside and outside the slot coater. The imbibition process in the slot coater is very complex and dynamic, with pressure pulses that, at the coating instants, are applied over very short times (on the order of milliseconds), accompanied (outside the slot coater) by longer periods (on the order of seconds) during which the fluid on the paper's top surface is driven into the paper by capillary forces. In the last stage the coating fluid is dried and solidified into its final position, within and on the top surface of the paper. We do not consider the drying stage and restrict ourselves to only the imbibition process.

To produce a high quality coating, it is necessary for the fluid to penetrate to some extent the pore structure of the paper. However, if the coating fluid penetrates too deeply into the paper, it can create severe problems for the coating operations and even the quality of the final product. The main

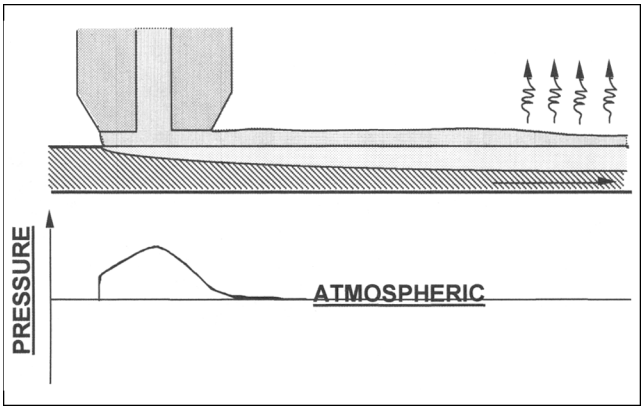

Figure 2. Pressure distribution in the slot coater (approximately parabolic) and outside the coater (atmospheric).

parameters that affect the penetration of the coating fluid into the paper are the structural characteristics of the paper, which are its porosity, pore-size distribution, pore connectivity, the shapes of the flow channels between the fibers, and the physical properties of the coating fluid which are its contact angle with the surface of the paper, both internal and external, and its surface tension and viscosity. Other parameters that influence this process are the velocity of the web during coating and the convective pressure profile in the slot coater which is applied to the top surface of the paper.

The economics of these products also plays an important role in this process. One requires that: (1) processing speeds be maximized; (2) the cost of the materials used in the process be reduced or minimized; while (3) the quality of the product be maintained at some desirable level. Reduction of the materials' cost can be achieved by reducing the amount used in the coating, but also by reducing the basis weight, or the density of the paper grade used, that is, by using papers that have higher porosities or those that have not been conditioned for subsequent coating by the application of a filler layer. However, these parameters act in opposite direction, and thus the developer of a new product must carefully optimize the parameters while improving the product quality and reducing its cost. Use of a more porous paper, or of one which has not been pre-conditioned for coating, requires utilizing more coating materials in order to achieve a continuous, high quality coating on its surface. However, under these conditions, the coating fluid may tend to penetrate deeper into the paper, bypassing some of the fibers near the top surface. On the other hand, if one wishes to minimize the amount of coating, one can resort to the use of denser papers, or of pre-coated papers, both of which are more expensive. In addition, the desire to coat at higher speeds often results in higher pressures at the applicator point which can, however, be a major driving force for flow of the coating fluid into the paper. Thus, in order to control the quality of the paper's coating, a deeper understanding of this phenomenon and the role of all the factors that can influence it are required. One major goal of this article is to investigate the effect of these parameters on the coating process.

Because of the many parameters that affect this process, and due to the complexity of the process itself, developing a model that can accurately describe the process is highly desirable, since one can employ such a model to explore many scenarios in which different types of paper and the coating fluid are used together with various web speeds in order to understand how they influence the imbibition process during coating, and hence direct the effort for improving the quality of the product and the economics of the process to the critical parts of the process. The experimental investigation of the same would, on the other hand, be an insurmountable task as there are a great variety of papers with various microstructures. Although such experiments are necessary and provide significant insight into the process, careful selection of the experiments to carry out becomes much more efficient and cost-effective with the guidance of the model.

To our knowledge, despite its great industrial importance, only very limited effort has so far been dedicated to modeling this phenomenon. Even then, almost all of the previous studies employed continuum models with several phenomenological coefficients, and represented the paper either by a contin-

uum characterized by an effective permeability and porosity estimated experimentally, or represented the paper's microstructure by a bundle of parallel capillary tubes—a one-dimensional (1-D) model (see, for example, Lyne and Aspler, 1982; Oliver, 1982; Oliver et al., 1991; Dantino and Marmur, 1994; Selim et al., 1997; Poulin et al., 1997; Hayes et al., 2000). The phenomenological models suffer from the fact that at least some of the coefficients that are used in the governing equations are simply ad-hoc parameters that have no clear physical meaning; they are used to force the models' predictions to agree with a specific set of experimental data. However, if such models with the same adjusted parameters are used for predicting another set of experimental data, they usually fail to provide accurate predictions. Models that represent the paper as a bundle of parallel capillary tubes cannot obviously be hoped to be predictive, since the microstructure of any paper is too complex to be presented by a 1-D model. There are only a few notable exceptions to such models. Pan et al. (1995) used small 3-D pore networks for representing the microstructure of the paper, and studied drying of the paper after it had been coated by the coating fluid. Qi and Uesaka (1996) and Koponen et al. (1998) represented the microstructure of the paper by realistic models of fibers and the channels between them, and employed the lattice-Boltzmann method (for reviews, see, for example, Sahimi (1993, 1995); Rothman and Zaleski (1997) to study flow of a liquid in the paper. However, their study was limited to computing the effective permeability of the paper; they did not consider the coating process that we study in this article.

The first effort of its kind is described for modeling the flow of a coating fluid into a porous substrate—a printing paper—in which the parameters and the boundary conditions are representative of a high-speed coating process. We develop a pore network model for the web (moving paper), and employ a novel model for imbibition of the coating fluid into the paper under both dynamic and capillarity-dominated conditions. We then study the effect of the various parameters on imbibition of the coating fluid in the paper.

In what follows the pore network model is described that we use for representing the microstructure of the paper to be coated. The model of the imbibition process, under both dynamic and capillarity-driven conditions, is then described. Next, the results are presented of extensive computer simulation of imbibition of the coating fluid in the paper and the effect is studied of the various parameters on this phenomenon. A summary also discusses how the model can be improved.

Model of the Paper

The first step in simulating imbibition of the coating fluid into a paper involves modeling the microstructure of the paper itself. The complex fiber network of a paper and the pore space between the fibers are highly difficult to describe exactly. The fibers themselves contain very tight pores into which a fluid can diffuse and/or flow. Since we are considering an imbibition process, the fibers' pores and throats can, in principle, be invaded by the (coating) wetting fluid, since during imbibition the invading fluid invades the *smallest* throats. However, we ignore the fibers' pore space, because: (1) the typical time scale for diffusion and/or flow of the invading fluid into the fibers is much larger than the time scale for the coating process and the subsequent drying of the coating layer; (2) the molecular size of the invading fluid may be too large to allow its penetration into the fibers' pore space. Therefore, we assume that the fibers are nonporous materials. Then, a realistic model of the pore space of a paper can be developed in terms of a network of flow passages *between* the fibers through which the coating fluid flows. These passages are represented by cylindrical capillaries or sheet-like channels called throats. The pores are where the throats intersect each other. The local coordination number of the network—the number of the throats connected to the same pore—is a stochastic variable which depends, among other things, on the density of the fibers, that is, the number of fibers per unit volume of the paper. The pore space can, however, be characterized by an average coordination number which we treat as one parameter of the model. The pores' and throats' walls also have rough surfaces with nonuniform compositions and wettability, but, for now, we ignore such complications. The effective radius of the throats is selected from a representative statistical distribution. The effective size of a pore is typically much larger than those of the throats that are connected to it. Thus, we first assign the effective radii of the throats. Then, for each pore, the effective radii of the throats that are connected to it are examined. Since the effective size of the pore must be at least as large as the size of the largest throat which is connected to it, we take the effective radius of the pore of be $mr_{\max}$, where m is a parameter which can take on any value, but, typically, $1 \le m \le 2$, and $r_{\max}$ is the effective radius of the largest throat connected to that pore. Because the fibers are distributed stochastically, the topology of the pore space of a paper is highly disordered, such that the local coordination numbers are statistically distributed. However, simulations of transport processes in topologically random networks (Jerauld et al., 1984) have shown that regular networks are often quite adequate for representing the disordered pore space of a porous material, if the coordination number of the regular network is the same as the average coordination number of the random network. Computations with regular networks also require much less computer times than those for random networks. Thus, we assume in this work that the pores and throats of the paper's pore space are represented by the sites and bonds of a simple-cubic network, respectively, which means that the coordination number of the underlying network is $Z = 6$. This model also affords us the flexibility of generating random networks using the cubic network as the underlying structure. If, for example, we wish to represent the paper's pore space by an average coordination number $\langle Z \rangle \le Z = 6$, then we first delete a randomly-selected fraction p of the throats, that is, we set their effective radii to be zero, such that

$$p = 1 - \frac{\langle Z \rangle}{Z}. \tag{1}$$

The resulting network has a random topology (connectivity) with an average coordination number $\langle Z \rangle$. In principle, the mean coordination number of the throat in the macroscopic flow direction is not the same as that in the planes perpendicular to the flow direction. However, we ignore this complication in this article because experimental data characteriz-

ing the difference between the two coordination numbers are not available yet.

Next, the throat size distribution $f(r_t)$ must be specified. Several attempts have been made in the past for measuring $f(r_t)$. When we began this study, we spent a considerable amount of time trying to measure $f(r_t)$ by the conventional methods. However, conventional methods of measuring $f(r_t)$ are not useful for papers. Nitrogen adsorption, a standard method for measuring pore-size distribution of porous materials, is not suitable for papers since their throat sizes are too large; they vary typically from submicron to microns, whereas nitrogen adsorption is useful if the effective throat sizes are in the nm range. Mercury porosimetry, another heavily-used method, destroys the paper. These are other methods that are claimed (Matthews et al., 1995, 1997) to be useful for measuring $f(r_t)$; however, they provide only qualitative information. Other attempts in this area (Deng and Dodson, 1994; Dodson and Ng, 1994; Dodson and Sampson, 1995; Räisänen et al., 1997), despite being very interesting, cannot provide direct information on $f(r_t)$. We thus realized that no quantitative method of measuring the size distribution of the throats was available yet. This motivated us to develop a novel method for measuring the distribution $f(r_t)$; the work is ongoing and its results will be reported in a future paper. On the other hand, it is well-known that is most porous materials the throat-size distribution is not Gaussian and symmetric, but skewed. Therefore, we assumed that the throat-size distribution can be represented by the following distribution function

$$f(r_t) = \frac{r_t - r_{\min}}{(r_{\text{ave}} - r_{\min})^2} \exp\left[-\frac{1}{2}\left(\frac{r_t - r_{\min}}{r_{\text{ave}} - r_{\min}} \right)^2 \right], \quad (2)$$

where $r_{\min}$ and r_{ave} are the minimum and average throat radii, respectively. Experimental information for $r_{\min}$ and r_{ave} is scarce. In our simulations we typically used a minimum and average throat radii of about 0.05 μm and 0.5 μm, respectively, but also treated them as the parameters of the model (see below). These values were deduced from analysis of scanning electron microscopy of the papers' cross sections. Hellén et al. (1997) proposed an exponentially decaying size distribution

$$f(r_t) = r_0^{-1} \exp(-r_t/r_0), \quad (3)$$

for the throat sizes, where r_0 is a constant. Over much of the range of possible values of r_t, distributions 2 and 3 produce similar values of r_t, except that, since Eq. 3 does not contain a minimum throat radius $r_{\min} > 0$, it predicts that the throats with $r_t \to 0$ are also the most abundant. While this may be true if the sizes of the extremely small throats in the fibers are also included in the distribution, the relevance of Eq. 3 to the process that we wish to model was not clear to us, as we ignore transport of the coating fluid into the fibers, and therefore we opted not to use Eq. 3.

Because of its fibrous structure, the pore space of a paper is anisotropic. How to characterize this anisotropy has been discussed in detail by Scharcanski and Dodson (1995). For example, the throats' length in the z-direction, the direction of macroscopic flow, are much shorter than those in the xy planes perpendicular to the flow direction. Moreover, the channels that run more or less parallel to the fibers are much longer than those that intersect them. Therefore, a direction-dependent throat length is the simplest measure of anisotropy; we used this in our simulations. We thus assumed that the lengths of the throats in the x-, y-, and z-directions are ℓ_x, ℓ_y, and ℓ_z, with $\ell_x \gg l_z$ and $\ell_x > \ell_y$. One important parameter that influences the quality of the coating process is the paper's thickness, which is also measured easily. Using this information, the length of the throats in the macroscopic flow direction, that is, the z-direction, can be adjusted once the network's linear size L_z in the z-direction is fixed. In the simulations a specific size of the network representing the web with dimensions $L_x \times L_y \times L_z$ was used, where L_x, L_y and L_z represent the number of nodes (pores) in the corresponding directions, and $L_x = L_y \gg L_z$. With such constraints, a series of preliminary simulations were carried out in order to select those values of L_x, L_y, and L_z which produce simulation results that were comparable with those obtained with larger networks. We found that $L_x = L_y = 40$ and $L_z = 4$ are adequate.

During the imbibition process, the paper may deform (by swelling first and then shrinking). The deformation would then distort the initial microstructure of the paper. The effect of the deformation has been investigated before within a continuum model (Chen and Scriven, 1990). Taking into account the effect of deformation will make the computations highly complex since, in effect, one must couple the Navier equations, that govern the distribution of the stresses and displacements in the deformable body, to the flow equations. In this article we neglect the effect of deformation because, according to our industrial partner, such effect does not seem to be significant since the fast imbibition process takes place at such short time scales that does not allow the paper to deform significantly.

Dynamic Boundary Conditions

The paper sample moves in the x-direction and passes through the slot coating area in which a convective (flow-driven) pressure is applied on its top surface, which is the liquid applicator point—the "pressure bell" (see Figure 1). The applied pressure is an important boundary condition for the flow of the coating fluid into the paper, and is, in practice, one of the most important factors that determines the success or failure of the entire coating process. Therefore, effort must be made to evaluate this pressure distribution as a function of the various parameters of the system, which are the applicator type and geometry, the coating fluid viscosity, the amount of the applied material, and the speed of the coating operations.

Finite-element analysis has been used for many years to evaluate flow and pressure fields of coating flows for such technologies as slide coating, curtain coating, blade coating, slot coating, roll coating, and others. In this approximation the flow at the applicator is coupled with the flow into the porous medium only by the pressure, which is applied to the pore space, in the form of a boundary condition. In the present case we have used the example of slot coating and applied numerical methods similar to the one described by Sartor (1990). The nondimensional Navier-Stokes system, coupled with the equations describing the free surfaces, were

Table 1a. Reynolds, Capillary, and Stokes Numbers, and Web Speed used in Calculating Convection-Driven Pressure Distributions

Case	v (m/min)	*Re*	*Ca*	*St*
1	100	1.19	2.24	2.10×10^{-4}
2	300	3.57	6.72	7.00×10^{-5}
3	400	4.76	8.96	5.25×10^{-5}

Table 1b. Fitted Coefficients for the Parabolic Pressure Distribution*

Case	a_1	b_1	c_1
1	−36,269	160,526	−6,834.2
2	−108,567	493,058	−42,786
3	−145,008	652,356	−46,922

*$P(x) = a_1x^2 + b_1x + c_1$, where P is in Pa and x in mm.

Table 1c. Fitted Coefficients for Parabolic Pressure Distribution*

Case	a_2	b_2	c_2
1	-1×10^{11}	3×10^{8}	−6,834.2
2	-3×10^{12}	2×10^{9}	−42,786
3	-6×10^{12}	4×10^{9}	−46,922

*$P(t) = a_2t^2 + b_2t + c_2$, where t is in s and P in is Pa.

integrated with a finite-element mesh of 600 biquadratic elements for the flow velocity and linear basis functions for the pressure field. The resulting set of nonlinear algebraic equations was solved by the Newton-Raphson method. The calculations were carried out for three distinct cases, each of which corresponded to a particular value of the web speed v. In this way, the Reynolds number, the capillary number $\mathrm{Ca} = \eta v/\sigma$, the ratio of the viscous and interfacial forces (where η is the fluid viscosity and σ the surface tension), and the Stokes number $\mathrm{St} = g\rho L^2/\eta v$, the ratio of the gravitational and viscous forces (where ρ is the fluid density and L a characteristic length scale), were varied. Under these conditions, we could simulate the flow of the coating fluid at web speeds varying from 100 m/min to 400 m/min. The specific values of the parameters are listed in Table 1a, 1b, and 1c.

From the solution of the Navier-Stokes equations, the three convection-driven pressure distributions, to be used as the boundary condition at the top surface of the paper, were determined. The results are shown in Figure 3. In the simulations the pressure varies with x according to such distributions, where x is the coordinate along which the paper moves at a constant speed v. For the sake of convenience, the pressure distributions were fitted to the following general form

$$P(x) = a_1x^2 + b_1x + c_1, \tag{4}$$

which, as Figure 3 indicates, provide accurate fits of the distributions. Table 1 also lists the resulting fitted coefficients a_1, b_1, and c_1 for the three cases. Note, however, that any other pressure distribution can be used, since $P(x)$ is an input parameter of the simulator. The pressures at the network's nodes on its top surface vary in the x-direction according to Eq. 4. For a given x, all the nodes in the y-direction (perpendicular to the x-direction in the xy plane) have the same pressure. Since the web moves at a constant speed, at any time t, one has $x = vt$, and therefore the coordinate x of a node can be calculated easily at the time t, from which the corresponding pressure at that x is computed using Eq. 4. Table 1 also provides the coefficients for the three cases if Eq. 4 is rewritten in terms of $t = x/v$, namely, $P(t) = a_2t^2 + b_2t + c_2$. Figure 4 compares the numerical results with the fitted equations. As can be seen, unlike $P(x)$, there are significant differences between the broadness of the three $P(t)$.

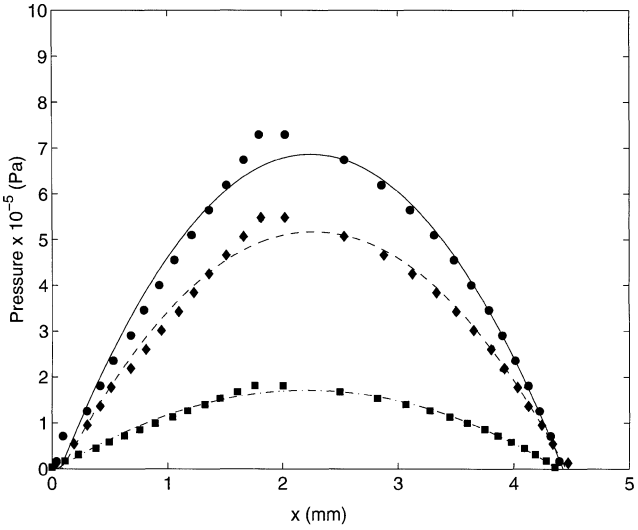

Figure 3. Convection-driven pressure distribution $P(x)$ calculated numerically (symbols) and their fits to Eq. 4.

The results are, from bottom to top, for Cases 1, 2 and 3 (Table 1).

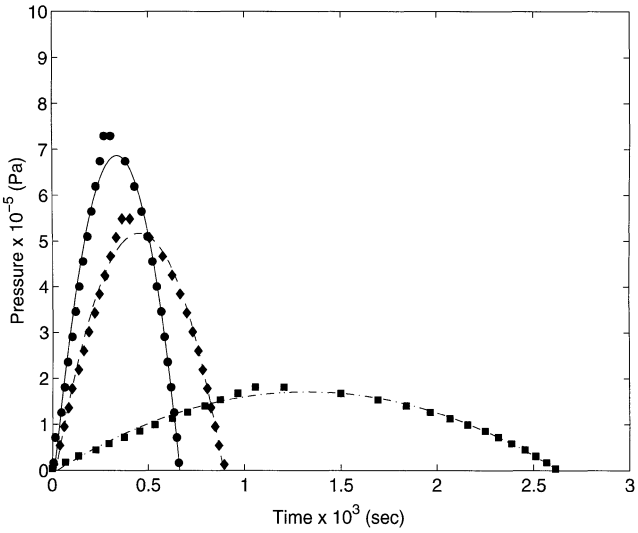

Figure 4. Time dependence of the convection-driven pressure distribution $P(t)$.

Symbols are the same as in Figure 3.

Imbibition Model During Coating

We assume that the coating fluid is Newtonian. This is only an approximation, as the coating fluid, which is typically an organic emulsion, is in fact a highly non-Newtonian fluid. However, aside from simple models of non-Newtonian fluids, such as the power-law model (Poulin et al., 1997), which itself is only an approximation to the true rheology of the coating fluid, it is not clear what rheological model can describe the coating fluid. Moreover, knowledge of how a Newtonian fluid imbibes the paper is a prerequisite in trying to understand more complex situations.

At the beginning (time $t = 0$) of the process, the network (the pore space of the paper) is filled with the nonwetting fluid (NWF), that is, air. Because air's viscosity is much less than that of the coating fluid, the pressure in the air phase is essentially constant. Therefore, we assume that the pressure in the air phase is constant and atmospheric, and compute only the pressure distribution in that part of the pore space that is occupied by the coating fluid. To calculate this pressure distribution, all the pores on the top surface are filled by the wetting fluid (WF), that is, the coating liquid. Assuming laminar flow in all the throats, the volumetric flow rate q in each throat is given by

$$q = \frac{\pi r_t^4 \Delta P}{8\eta l_t} \tag{5}$$

where r_t is the throat's effective radius, ΔP is the pressure drop along the throat, η is the coating fluid's viscosity, and l_t is the throat's length ($l_t = \ell_x$, ℓ_y, or ℓ_z). It will not pose any conceptual or computational difficulty if we assume that the throats have sheet-like structure, and use the corresponding well-known expression for q (in which case q is proportional to r_t^3), if we interpret r_t as the half-width of the throat. For the throats at the interface between NWF and WF phases, the throat capillary pressures

$$P_{ct} = \frac{2\sigma \cos\theta}{r_t}, \tag{6}$$

are also added. The coating fluid then imbibes into the network and tries to penetrate into the smallest throats first. Those throats that can be invaded by the WF are called the allowed throats. However, some of these throats are surrounded by larger ones into which the WF will not enter, implying that not all of the allowed throats will actually be penetrated by the coating fluid. Therefore, of all the allowed throats, only a fraction of them is actually accessible to the coating fluid. During the entire simulation, the trapped pores and/or throats, that is, those that are filled by air and surrounded completely by the WF, are also identified. The untrapped air in the throats and pores which is displaced by the coating fluid is pushed out of the pore space from the two yz side planes.

At each time step, the coating fluid displaces the air and enters a pore or throat. The time for filling a throat or a pore is calculated. The Washburn equation (Dullien, 1992) is used to calculate the filling time of a throat

$$v = \frac{dl}{dt} = \frac{r_t^2}{8\eta l_t}\left[\left(\frac{2\sigma\cos\theta}{r_t}\right) \pm \rho g(z - z_0)\right], \tag{7}$$

where dl is the distance that the interface between the NWF and WF travels in the time dt, g is the gravitational acceleration, z the vertical distance of the interface from the top surface (the entrance of the coating fluid to the pore space), z_0 is a reference point, and the signs $\pm$ depend on whether the interface is moving in the direction of, or opposite to, the gravity, respectively. Of course, depending on whether the interface is moving in a horizontal or vertical throat, the Washburn equation must be modified slightly. The WF can also flow in a throat as thin films that are attached to its internal surface. However, since the time scale for film flow is typically much larger than the typical time scale for the coating operations, we ignore film flow. Including the effect of flow of thin WF films is, in principle, possible (see, for example, Blunt and Scher, 1995; Hashemi et al., 1999), but doing so would only make the computations much more complex without adding much to the physics of this problem.

We should point out that the contact angle that we use in the simulations is the *static* contact angle, the use of which for the imbibition simulations outside the slot coater, where fluid penetration into the pore space is driven only by capillarity, is justified. However, in the slot coating area where the fluid penetration into the paper is a *fast* imbibition process, we should, in principle, utilize the *dynamic* contact angle θ_d. Experimental and theoretical work (see, for example, Cox (1986), de Gennes (1988), Stokes et al. (1990)) indicates that the dynamic contact angle in a pore (cylindrical tube) depends on the fluid velocity in that pore. For example, from their experimental observations and data, Stokes et al. (1990) found that

$$\cos\theta_d - \cos\theta_a = aCa^b, \tag{8}$$

where θ_a is the *advancing* contact angle, which in their experiments was about 65′. In Eq. 8 the capillary number Ca is based on the fluid velocity v in the throat, which, of course, changes from throat to throat, and also varies as the dynamic boundary condition at the paper's top surface changes with the process time. a and b are two constants, and in particular Stokes et al. (1990) found that $b \simeq 0.4$. Other authors have suggested different values for b. The most important implication of Eq. 8 is that the dynamic contact angle depends nonlinearly on the fluid velocity in the pore. We are currently studying the effect of the dynamic contact angle on the imbibition process, the results of which will be reported in a future article.

To calculate the pressure distribution in the network, we use the fact that the net amount of the fluid entering a pore must obey detailed mass balance, implying that

$$\sum_{ij} q_{ij} = 0 \tag{9}$$

where q_{ij} is the volumetric flow rate in the throat ij which is connected to pore i. The sum is over all the throats ij for which $q_{ij} \neq 0$. Using Eq. 5 and writing down Eq. 9 for every

pore (node) of the network results in a set of simultaneous equations for the nodal pressures which is solved by the conjugate-gradient method. After the pressure distribution is calculated, the flow rate and the time for filling all the interfacial elements are also computed. Since the paper is moving, the boundary conditions at the top surface change with the process time. As time increases, the set of the throats that are filled with air and are invaded by the coating fluid also grows, and, therefore, the pressure distribution in the set of the invaded pores and throats also changes. Thus, the pressure distribution in the network must be continuously updated with the process time. Hence, a basic time step Δt is needed for updating the pressure distribution. Since the web speed is typically large, Δt must be selected carefully so that the effect of the dynamic changes in the pressure distribution on the imbibition of the coating fluid into the paper can be modeled properly. If Δt is taken to be too large, then the effect of the continuous changes of the pressure distribution at the top surface cannot be taken into account. On the other hand, if Δt is selected to be too small, then the cost of the computations will be very large, since one must solve the set of the equations for the nodal pressures a very large number of times. After some preliminary simulations and studying the results for a few values of Δt, we developed the following method for selecting Δt. Each time the pressure distribution is computed, we take Δt to be the minimum time to fill a pore and 10% (in length) of a throat connected to it, where this filling time is calculated for all the pores and throats that are at the interface between the coating fluid and the air. Since the filling time for a throat is proportional to r_t^2, the implication is that the smallest throats are filled first, which is the essential physics of the imbibition process.

The coating fluid then moves into the selected throat (and pore) and fills it up to the specified length. Over the same time step Δt, the fluid also invades the other throats that are connected to the interface and fills smaller portions of them. Since the velocities of the fluid in such throats are known, the length of these portions are calculated for all the interfacial throats and the fluid is moved into these throats to fill these segments. The convective pressure at the top surface is

Table 2. Model Parameters Required for the Simulations

Parameter	Value
Min throat radius r_{min}	0.05 μm
Avg. throat radius r_{ave}	0.1 and 0.45 μm
L_x	40
L_y	40
L_z	4
Thickness of paper	50 μm
Network coordination no.	6.0 and 5.0
Vis. of coating liquid	5, 10, and 20 cp
Dens. of coating fluid	1 g/cm^3
Surface tension	30, 40, and 50 dyne/cm
Contact angle	10°, 20°, and 30°

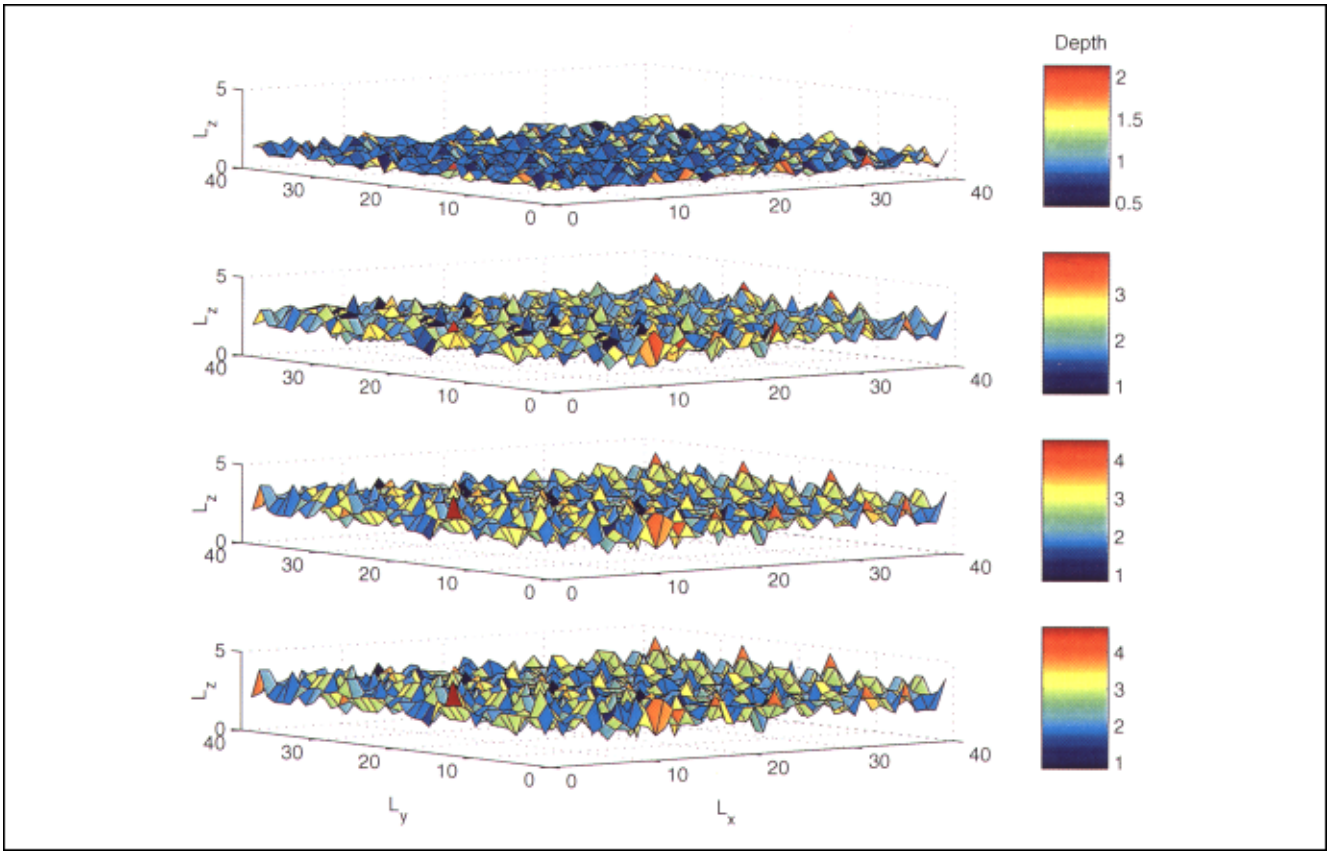

Figure 5. Spatial distribution of the coating fluid in a paper at four different times.

Time increases from top to bottom.

now updated, because, during the time Δt, the paper has moved a certain distance in the slot coater. This provides the new boundary condition at the top surface with which the pressure distribution in the pore space is recalculated, the time Δt is selected, the coating fluid is moved into its new positions in the pore space, and so on. The simulations continue until either the coating fluid reaches the bottom surface of the paper, that is, the throats filled with the fluid form a sample-spanning percolation cluster, or a specified length L of the paper has passed the system. L is taken to be the sum of the length L_c of the paper in the convective-pressure zone and a distance nL_x, that is, $L = L_c + nL_x$. After some preliminary simulations in which we varied n, we found that selecting $n = 3$ provides a long enough L for the total length of the paper to be used in the simulations.

The simulations were carried out for two different papers used by Avery Dennison Corporation, and the three pressure distributions listed in Table 1. There was very limited information about the papers' characteristic parameters, such as their typical throat size and length, and thickness. No information was yet available about the coordination number Z of the papers' pore space, and thus we treated Z as a parameter of the simulations. In addition to the microstructural parameters of the papers, and the pressure distribution on the top surface of the web, one must also supply to the simulator the physical properties of the coating fluid. These properties are given in Table 2. Their effect on the imbibition process was also studied (see below).

Results

Of particular interest to us are the average and the maximum penetration depths of the coating fluid in the paper for each case (paper type and the convection-driven pressure distribution) that we studied. Thus, in what follows we evaluate the performance of the coating process under various conditions in terms of the average and maximum penetration depths of the coating fluid in the paper.

Effect of microstructural characteristics of the paper

Figure 5 shows the spatial distribution of the penetration depths of the coating fluid in a paper at four different times during imbibition with the top one showing the results at an early time and the bottom one presenting the same at the end of the process. The time-dependence of the average penetration depth of the fluid in the pore space is obtained by averaging the results shown in such panels for the particular time at which they are shown. The results shown in Figure 5 were obtained with $r_{\min} = 0.05$ μm, $r_{\text{ave}} = 0.45$ μm $\langle Z \rangle = Z = 6$, $\eta = 20$ cp, $\sigma = 40$ dynes/cm, and $\theta = 10°$, and Case 3 pressure distribution (Table 1) was used as the boundary condition at the top surface. As this figure indicates, the spatial distribution of the coating fluid in the pore space is highly inhomogeneous. The fluid has not invaded some parts of the pore space too deeply and has stayed close to the top surface, while, in other parts of the pore space, it has penetrated the

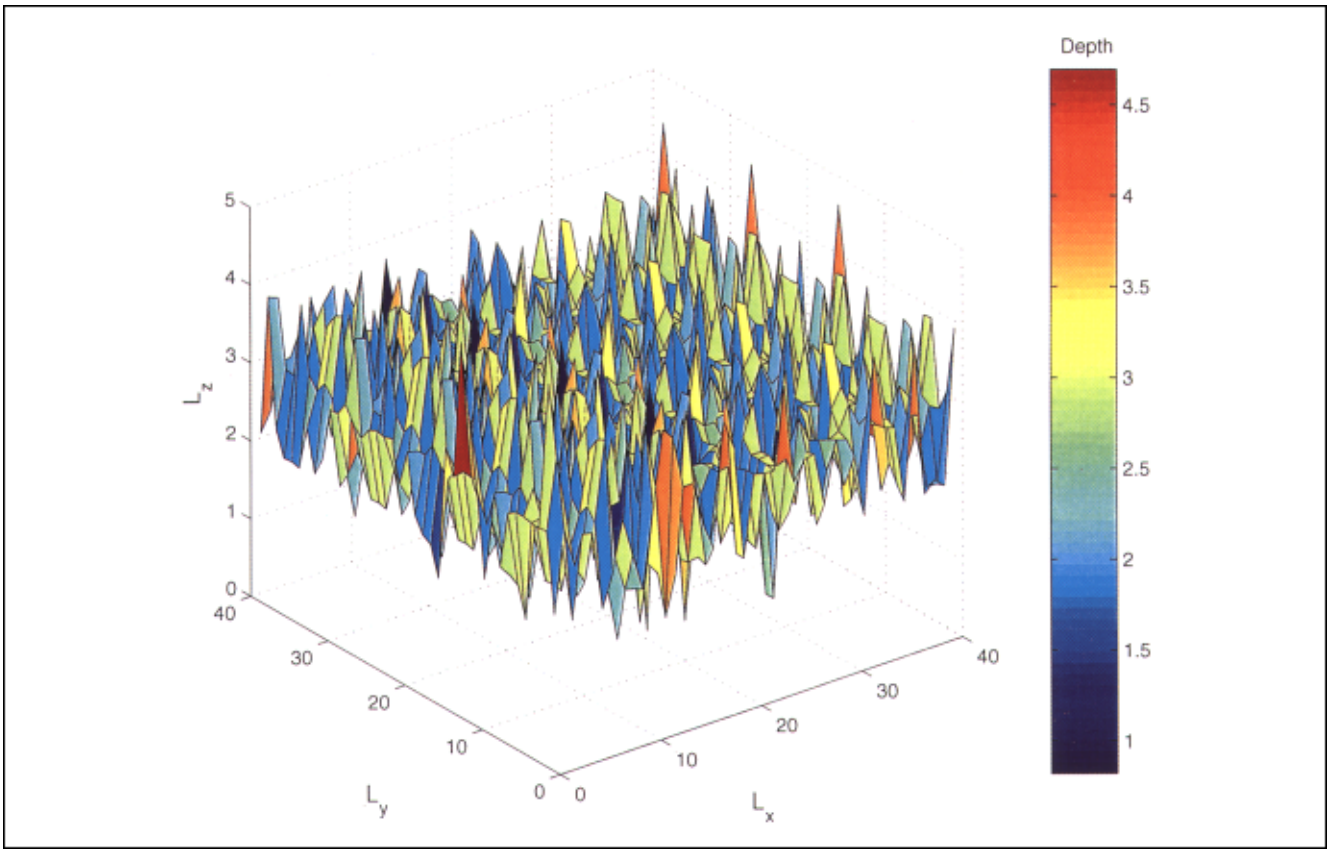

Figure 6. Example of the spatial distribution of a coating fluid in a paper with the fluid reaching the paper's bottom surface.

paper very deeply, but not so much that it has actually reached the bottom surface. Figure 6 shows the results at the end of the simulations with the same set of the parameters as those of Figure 5 except that $\eta = 5$ cp, and Case 2 pressure distribution was used as the boundary condition. In this case, the throats that are filled by the coating fluid have in fact formed a sample-spanning cluster and, hence, the fluid has reached the bottom surface of the paper. This is not desirable from a practical viewpoint. These results already indicate the strong influence of the coating fluid's viscosity and the convection-driven pressure distribution on the top surface. We shall come back to this point later in this article.

A series of simulations was carried out in order to understand the effect of the minimum throat size r_{min}. However, even large variations in r_{min} changes the throat size distribution only moderately, and, therefore, it is reasonable to expect, at most, weak changes in the average penetration depth of the coating fluid during the imbibition process. This is indeed the case (see Figure 7). In these simulations, we employed the Case 2 pressure distribution (see Table 1) with $r_{ave} = 0.1$ μm and $\langle Z \rangle = Z = 6$. The fluid's properties were $\eta = 10$ cp, $\sigma = 50$ dyne/cm, and $\theta = 10°$. The results for two cases with an order of magnitude difference between the two, $r_{min} = 10^{-3}$ μm and 10^{-2} μm, are compared. The average penetration depths have been normalized with the paper's thickness d. In this and the subsequent figures, the solid circle on the time axis indicates the time at which the paper has left the slot coater. Thus, if a curve that shows the time-dependence of the average penetration depth has been terminated at times smaller than what is indicated by the solid circle, it implies that the coating fluid reached the bottom surface of the paper *before* the paper left the slot coating area, and thus the simulation was stopped. As Figure 7 indicates, there is virtually no difference between the time-dependence of the average penetration depths for the two cases, and therefore for all the results that we discuss below we have fixed r_{min} at 0.05 μm.

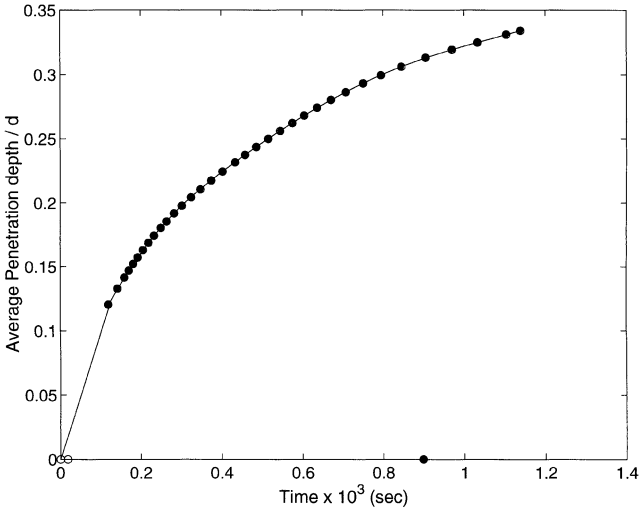

Figure 7. Effect of minimum throat radius r_{min} on the average penetration depth of coating fluid, normalized by the paper's thickness d.

The results are for $r_{min} = 10^{-2}$ μ (solid curve) and $r_{min} = 10^{-3}$ μ (circles).

Next, we study the effect of the average throat radius r_{ave} on the phenomenon. Variations in r_{ave} afford us the possibility of constructing and studying different paper microstructures, ranging from a very open pore space to a very tight one. If r_{ave} is close to r_{min}, the throat size distribution is narrow, and therefore the paper is relatively uniform but populated with small throats. For this limit, we used $r_{ave} = 0.1$ μm and found that the maximum throat size for this limit is typical about 0.8 μm. Increasing r_{ave} makes the throat size distribution broader and the paper more open and, hence, more heterogeneous. To simulate this type of microstructure, we used $r_{min} = 0.45$ μm, which yielded a maximum throat size of about 5 μm. The limited experimental data (based on SEM pictures) that were available for one of the sample papers indicated that its thickness was in the range 50–70 μm and its largest flow channel opening had a diameter of about 5–10 μm, in the same range that we used in our simulations (see Table 2).

The results for the two values of r_{ave} and three values of the surface tension σ (see Table 2), shown in Figure 8, indicate that this parameter has a crucial effect on the average penetration depth of the coating fluid. In these simulations we used $\langle Z \rangle = 5$, $\eta = 20$ cp, $\theta = 10°$, and Case 3 pressure distribution was employed as the boundary condition on the top surface. For the higher r_{ave}, the average penetration depth is also larger: Increasing r_{ave} creates a pore space which is more open and populated with a broad mixture of small and large throats. The smaller throats (in which imbibition takes place first) are connected to the top surface and possibly form a sample-spanning cluster from the top to bottom surface of the paper. This gives rise to flow channeling in the paper by which most of the coating fluid flows through the paper by an efficient (albeit undesirable from a practical view point) path of the small throats. As can be seen in Figure 8, beyond the time for exiting the slot coater (the solid circle on the time axis), the growth with process time of the average penetration depth of the fluid levels off and becomes essentially a constant. This is, of course, due to the fact that outside the slot coater the imbibition process is driven only by capillary forces which is much weaker than the applied convection-driven pressure in the slot coater. To understand these results better, we show in Figure 9 the time dependence of the maximum penetration depths of the coating fluid for the same systems as those of Figure 8. It is clear that, with the larger r_{ave}, the coating fluid has penetrated the pore space much deeper, and in fact had the paper not passed through the slot coater area (if, for example, the web speed v had been smaller), the fluid would have percolated through the sample and reached the paper's bottom surface. Figure 9 also indicates that there are discontinuities in the curves. These discontinuities are caused by the fact that, over certain periods of time, the coating fluid invades the throats and pores in the xy planes (perpendicular to the direction of the macroscopic flow) without advancing in the z-direction. As a result, the maximum penetration depth may not change over certain periods of time until the fluid resumes advancing in the z-direction.

If we reduce the viscosity of the coating fluid to 5 cp, but keep the rest of the parameters the same as those of Figures 8 and 9, we obtain the results shown in Figure 10. The quali-

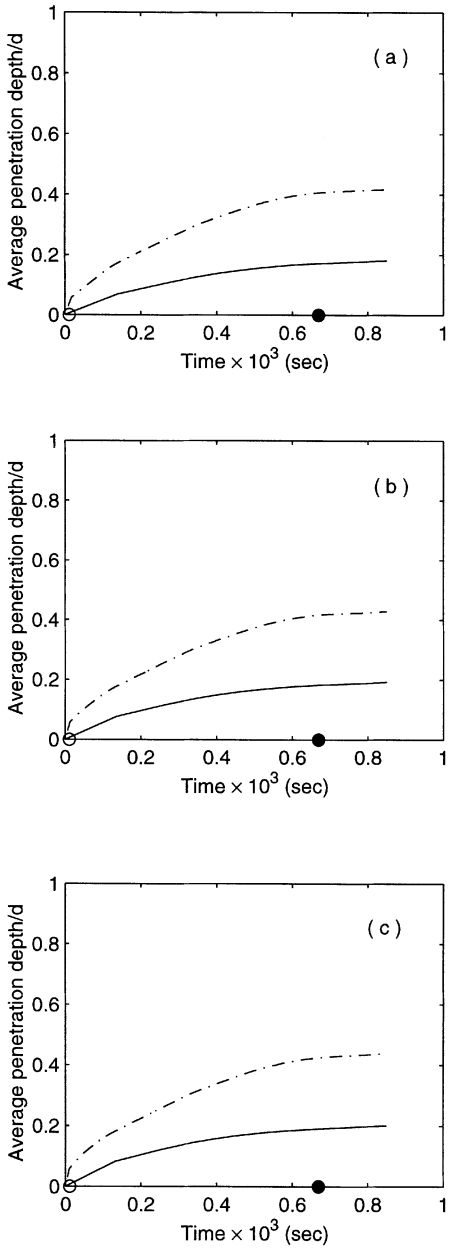

Figure 8. Effect of the average throat size r_{ave}.

Solid and dashed curves are for $r_{ave} = 0.1$ μm and 0.45 μm, respectively. The results are for $\sigma = 30$, 40 and 50 dyne/cm for cases (a), (b) and (c), respectively. The coating fluid's viscosity is 20 cp.

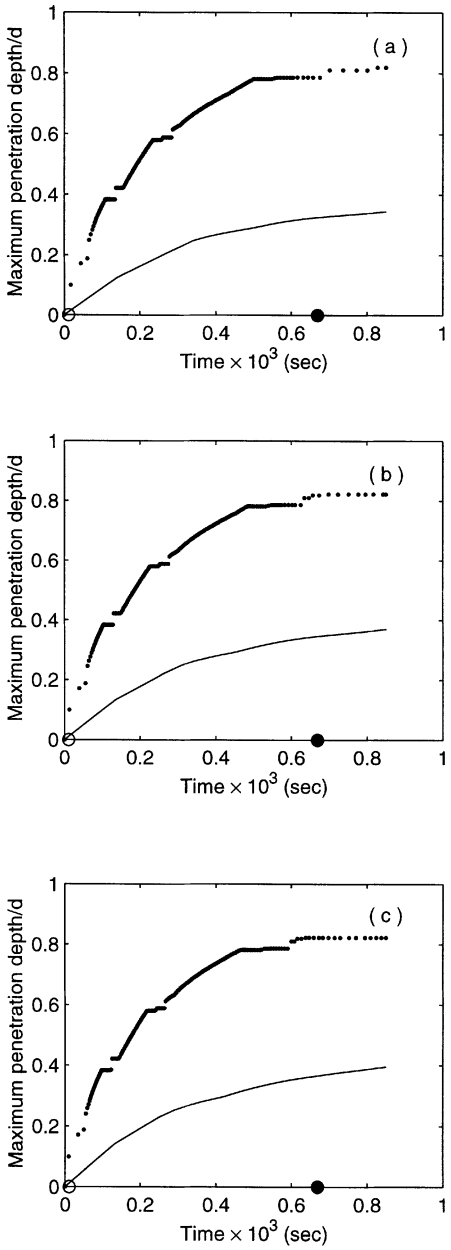

Figure 9. Effect of the average throat size on the maximum penetration depth of the coating fluids.

Symbols and parameters are the same as those in Figure 8.

tative patterns are the same for both cases, except that with the smaller viscosity and a larger average throat radius r_{ave} (the dashed curves in Figure 10), the coating fluid invades the paper much faster, so much so that it has actually reached the bottom surface of the paper (indicated by the fact that the dashed curves have been terminated before the time for exiting the coater).

Next, we consider the effect of the pore space connectivity on the process. The coordination number of the pore space provides us with information about its tortuosity. Lower coordination numbers indicate less connection between the throats and therefore higher tortuosities, implying that, for the same process time, the penetration depth for a paper with a low coordination number should be smaller than that of one with high connectivity, and our simulations indicate that this is indeed the case. Figure 11 presents the average penetration depths for three coordination numbers. In these simulations, we used $\eta = 10$ cp, $r_{min} = 0.05$ μm, $r_{ave} = 0.45$ μm, $\theta = 10°$, and Case 1 pressure distribution was utilized as the boundary condition at the top surface. The results are for the three values of the surface tension listed in Table 2. It is clear that the coordination number has a very strong effect on the average penetration depths. The results for all the

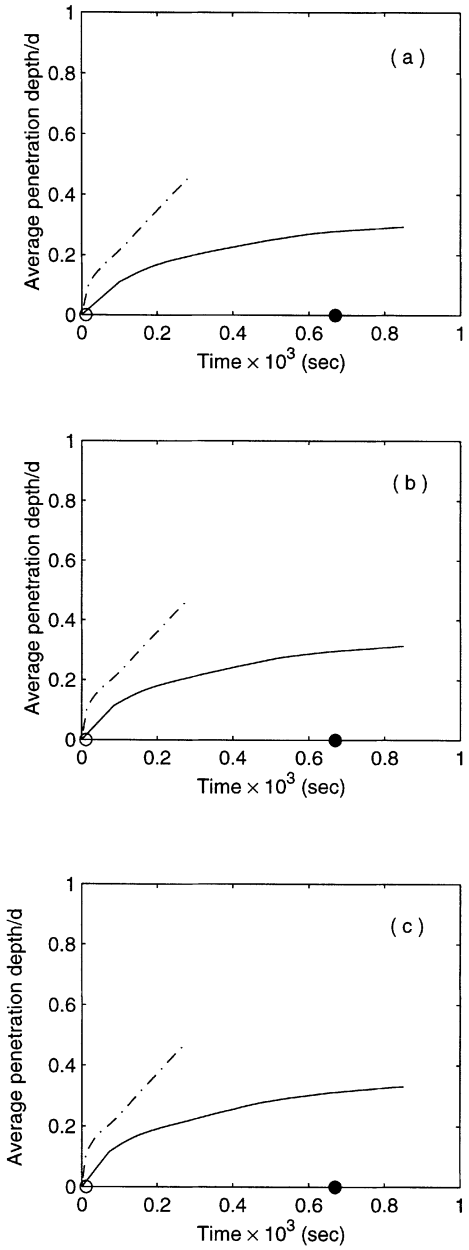

Figure 10. Same as in Figure 8, but for a coating fluid viscosity of 5 cp.

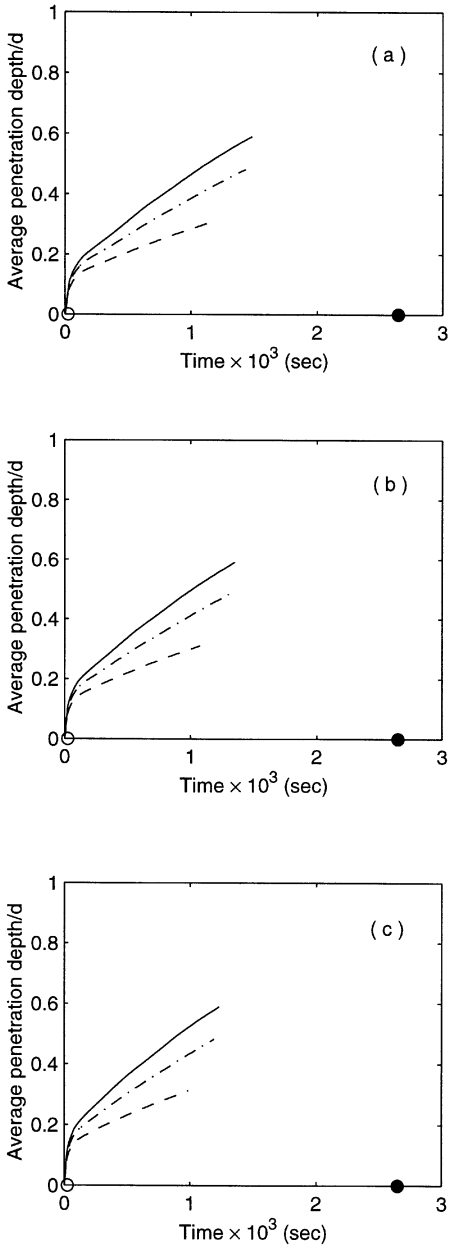

Figure 11. Effect of the mean coordination number $\langle Z \rangle$.

The results are, from top to bottom, for $\langle Z \rangle = 4$, 5, and 6, and $\sigma = 30$, 40 and 50 dyne/cm for cases (a), (b), and (c), respectively. The average throat radius is 0.45 μm.

cases shown in Figure 11 indicate that the coating fluid has reached the paper's bottom surface before the paper has left the slot coating area. If we reduce r_{ave} to 0.1 μm, then we obtain the results shown in Figure 12, indicating that, as one might expect, with a lower average throat size, the invasion of the paper by the coating fluid is restricted essentially to a region near the top surface. The difference between the three coordination numbers can be better understood if we look at the spatial distributions of the coating fluid in the pore space. Shown in Figure 13 are these distributions at the end of the simulations; the parameters of the model are the same as those of Figure 12. As can be seen, when the pore space is well connected, $Z = 6$, the spatial distribution of the coating fluid (top panel in Figure 13) is relatively smooth, as is expected from an imbibition process in a relatively homogeneous pore space. As we lower the average coordination number of the paper, the fluid's spatial distribution also becomes more inhomogeneous; see the middle panel for $\langle Z \rangle = 5$. For $\langle Z \rangle = 4$ (the bottom panel in Figure 13), the spatial distribution of the fluid is highly heterogeneous, as the low connectivity of the pore space makes the flow paths highly tortuous.

These aspects of the problem that we have discussed so far cannot be studied or predicted by a continuum model which is traditionally used by the engineers. In order to be able to

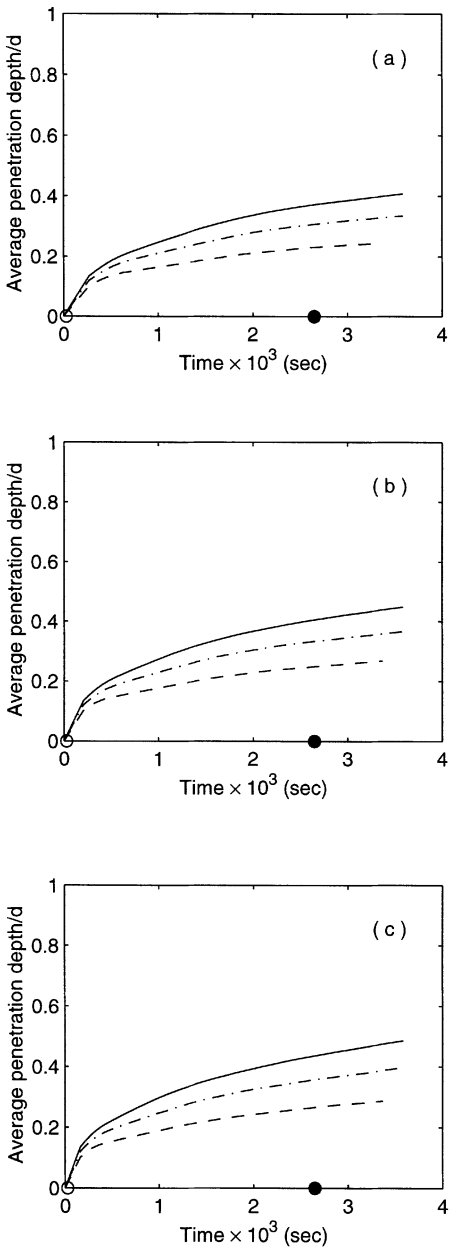

Figure 12. Same as in Figure 11, but for an average throat radius of 0.1 μm.

predict such effects, a detailed microstructural model of the type that we have used here is needed.

Effect of coating fluid's characteristics

We now consider the effect of the coating fluid's properties on the performance of the coating process. The first property whose effect we consider is the contact angle θ which is a measure of the fluid's ability for wetting a solid surface. When the coating fluid is completely wetting, $\theta = 0°$. However, as long as $\theta \leq 65°$, the fluid can be considered as wetting, in which case, as Eq. 7 indicates, varying θ causes only small changes in the penetration depths of the fluid. (For the typical fluids that are used in the coating processes, $\theta \leq 20°$.) This expectation is confirmed by the results shown in Figure 14, where we present the time-dependence of the average penetration depths of the coating fluid for three values of θ. In these simulations we used $Z = 6$, $\eta = 10$ cp, $r_{min} = 0.05$ μm, $r_{ave} = 0$ μm, Case 2 pressure distribution was utilized as the boundary condition at the top surface, and the results were computed for the three surface tensions listed in Table 2. As can be seen, the difference between the three cases is small. However, we must caution the reader that one possible reason for the insensitivity of our results to the contact angle is that our model is not really capable of taking into account the exact dynamics of wetting on the throats' surfaces. This inability is a characteristic of all such pore network models. In other words, in the context of a pore network model, all the fluids that are considered as wetting are treated essentially the same way, regardless of the exact value of their contact angle with the throats' surfaces. Moreover, as discussed above, one should use the dynamic contact angle in the simulations, the value of which varies from throat to throat, and also changes with the dynamic boundary condition at the top surface. There are more sophisticated microscopic models that can take into account such effects (see, for example, Cieplak and Robbins, 1990). However, these models are for unconsolidated porous media (such as a random sphere packing) and, due to their highly complex detail, are restricted to 2-D systems. This will of course not be the case if $\theta \geq 65°$. For $65° \leq \theta \leq 105°$, one is in the intermediate wettability regime (that is, no strong preference for wetting the throats' surface by either fluids), and for $\theta \geq 105°$ one must deal with a NWF. In such cases, however, the mechanisms of fluid penetration change drastically and the simulator must be revised.

The viscosity of the coating fluid is an important parameter in the coating process. A fluid with a higher viscosity moves more slowly in a porous medium than one with a lower viscosity since, over a given period of time, it penetrates the throats more slowly than a fluid with a lower viscosity. On the other hand, if the fluid viscosity is high enough, its penetration into the pore space is more or less uniform, since the interface between the displacing and displaced fluid (air) is completely stable and thus advancement of the interface in the pore space is uniform. In this case no fingering or channeling occurs. Thus, in practical terms, if the convection-driven pressure at the top surface is not too large, the fluid will not penetrate the paper all the way to its opposite face, which is desirable, because it first invades most of the throats in the *xy* planes (perpendicular to the direction of the macroscopic flow) and then tries to advance in the *z*-direction.

To see whether these qualitative observations are predicted by our model, all the parameters of the system were fixed, and only the viscosity of the coating fluid was varied. The results for the average penetration depths and the three values of the surface tensions (see Table 2), shown in Figure 15, confirm that the fluid viscosity has a strong effect on its penetration depth. In these simulations we used, $\langle Z \rangle = 5$, $r_{min} = 0.05$ μm, $r_{ave} = 0.1$ μm, and $\theta = 10°$. Case 3 pressure distribution was used as the boundary condition at the top surface. It is seen that, the smaller the fluid viscosity, the larger are the average penetration depths. If we fix all the parameters, but use an average throat size $r_{ave} = 0.45$ μm, we obtain the results shown in Figure 16. In this case, the average penetration depth of the fluid with the lowest viscosity is

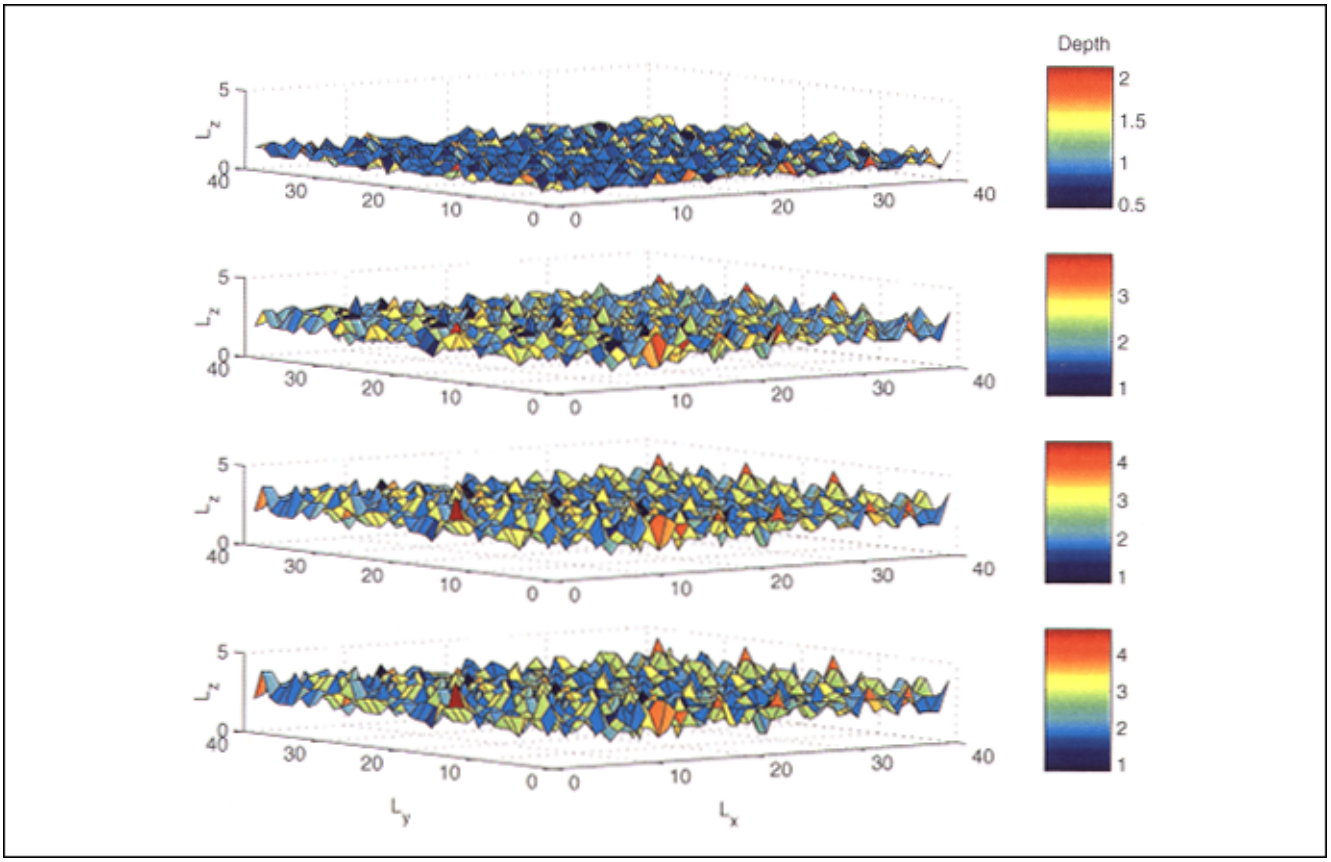

Figure 13. Effect of the mean coordination number $\langle Z \rangle$ on the spatial distribution of the coating fluid in the paper at the end of the simulations.

The results are, from bottom to top, for $\langle Z \rangle = 4$, 5 and 6.

about 50% of the paper's thickness. Moreover, as indicated in the figure, the coating fluid with the two lower viscosities has actually reached the paper's bottom surface before it has left the slot coater. From a practical viewpoint, these features are highly undesirable. However, by choosing a coating fluid with the right viscosity, one can control its penetration depth and prevent an unwanted outcome.

Surface tension σ of the coating fluid is also expected to have a direct effect on the imbibition process. Increasing σ also increases the capillary pressure P_{ct} (Eq. 6) at the interface between the coating fluid and the air, which then increases the penetration depth of the fluid, since, according to Eq. 7, the penetration depth l is directly related to σ. The simulation results, shown in Figure 17, verify this effect. In these simulations we used $Z = 6$, $r_{\min} = 0.05$ μm, $r_{\text{ave}} = 0.1$ μm, $\eta = 5$ cp, and $\theta = 10°$. At the boundary condition at the top surface, we used Case 2 pressure distribution. It is seen that with increasing surface tension the average penetration depth of the coating fluid also increases. If we keep all the parameters fixed, but increase the fluid viscosity to $\eta = 20$ cp, we obtained the results that are shown in Figure 18 which indicate that, as expected, the higher viscosity counters the effect of the surface tension and as a result, compared with the results shown in Figure 17, the average penetration depths decrease.

Effect of the dynamic boundary condition

The convective (flow-driven) pressure is applied at the top surface of the paper in the slot coating zone. If the applied pressure is much greater than the throat capillary pressures, then the convective pressure is expected to have a significant effect on the imbibition process and hence the coating operations; otherwise, it will have very little effect. The capillary pressure is directly proportional to σ and the inverse of the throat radius r_t. Therefore, for a paper with very small throat sizes, the pressure-driven convection does not affect the penetration depth of the coating fluid into the paper; this is roughly true for throat sizes that are approximately on the order of angstroms. If the throat sizes are large enough that the capillary pressures are much smaller than the (convective) pressure applied at the top surface, then the effect of the flow-driven pressure will be significant.

To check this, simulations were carried out for two different situations. First, the paper was moved in the slot coating area in which the convective pressure is applied. Later, the same paper with the same microstructural characteristics and the same fluid were used to simulate a spontaneous imbibition driven by capillary pressure alone. The results are shown in Figure 19. In these simulations we used $\langle Z \rangle = 5$, $r_{\min} = 0.05$ μm, $r_{\text{ave}} = 0.45$ μm, $\eta = 10$ cp, and $\theta = 10°$. The boundary condition at the top surface was Case 3 pressure distribu-

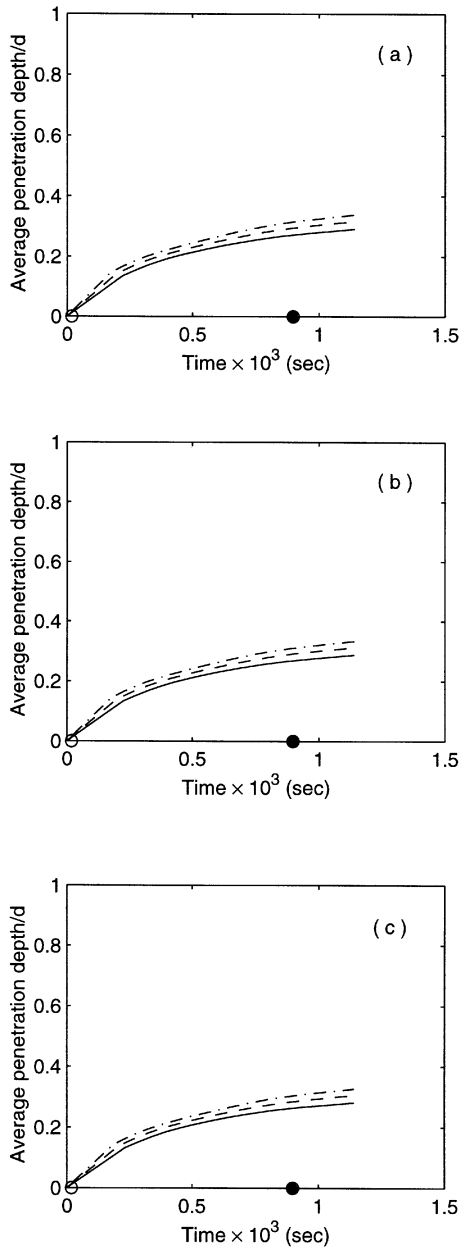

Figure 14. Effect of the contact angle θ.

The results are for $\theta = 10°$, 20° and 30° for cases (a), (b) and (c), and, from bottom to top, for $\sigma = 30$, 40 and 50 dyne/cm, respectively.

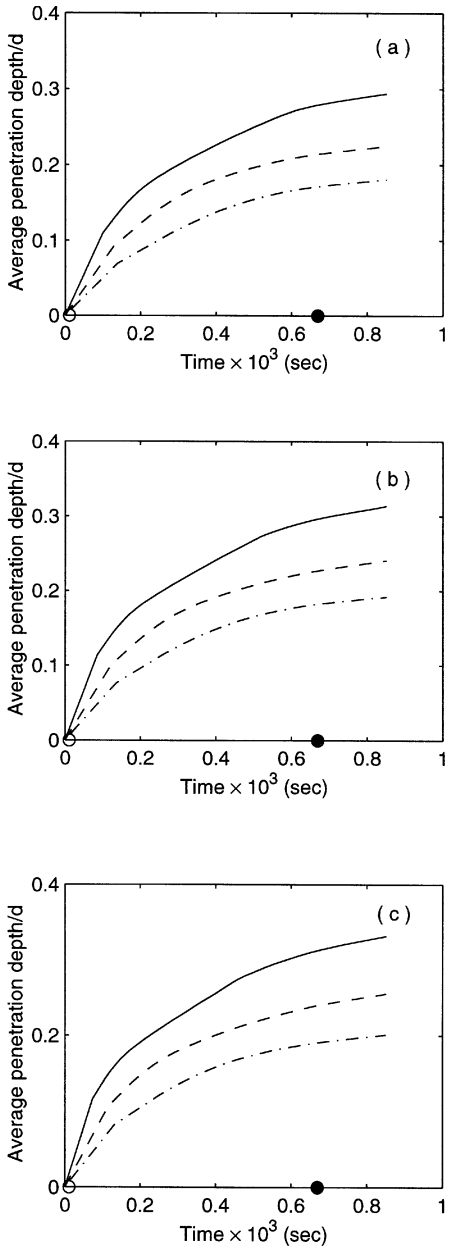

Figure 15. Effect of the coating fluid's viscosity η.

The results are, from top to bottom, for $\eta = 5$, 10 and 20 cp, and for $\sigma = 30$, 40 and 50 dyne/cm for cases (a), (b) and (c), respectively. The average throat radius is $r_{ave} = 0.1$ μm.

tion (see Table 1). It can be seen that the convective pressure has a strong effect on the coating process: The average penetration distances which result from applying the convective pressure is much larger than those obtained with capillarity-controlled imbibition. In fact, with the right parameters, this effect is so strong that the coating fluid passes through the paper.

Finally, we investigated the effect of the three convective pressure distributions, listed in Table 1, on the imbibition process. Using $Z = 6$, $r_{min} = 0.05$ μm, $r_{ave} = 0.1$ μm, $\eta = 10$ cp, $\theta = 10°$, and $\sigma = 30$ dyne/cm, we carried out three sets of simulations, each with one of the convection-driven pressure distributions listed in Table 1. The results are shown in Figure 20. As can be seen, the average penetration depths with Case 1 pressure distribution are significantly larger than those of the other two Cases. The results for Case 2 and Case 3 pressure distributions are close to each other, since their three controlling dimensionless numbers, namely, the Reynolds, capillary, and Stokes numbers, and also their web speeds are similar. The main culprit for the larger difference between Case 1 on one hand, and Cases 2 and 3 on the other hand is, of course, the web speed. For Case 1, the web speed is much smaller than those of the other two cases, thus providing the

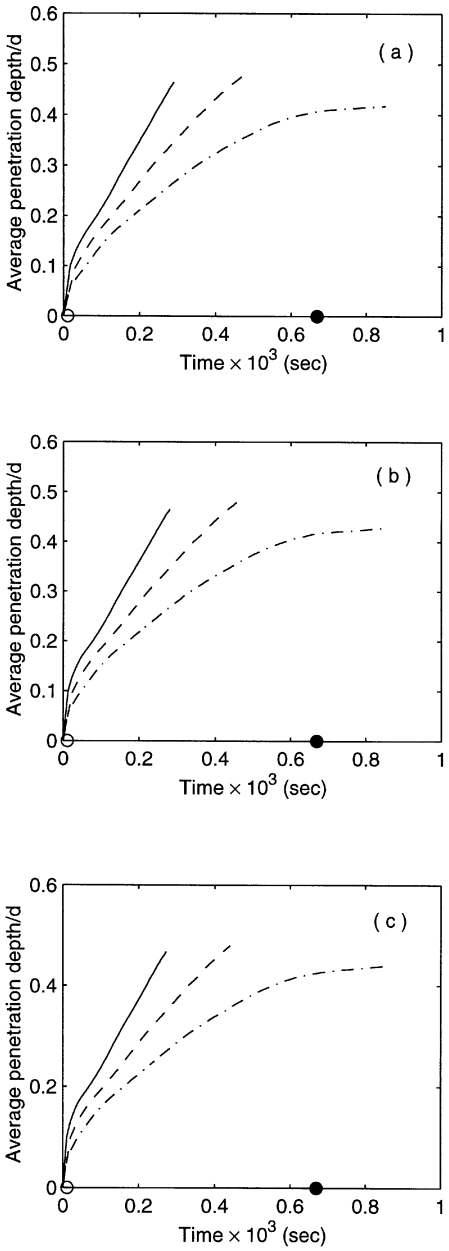

Figure 16. Same as in Figure 15, but for an average throat radius of $r_{ave} = 0.45$ μm.

coating fluid with ample time for penetration into the paper. Hence, the web speed, which can be easily designed or adjusted, is an important controlling factor during the coating process. However, it is not yet clear whether web speed will produce the same type of strong effect if the microstructural parameters of the paper, and, in particular, r_{ave} and $\langle Z \rangle$, are very different from those used in this study. Work investigating such issues is currently in process.

Summary

We have developed what we believe to be the first pore network simulator for studying the effect of paper microstructural parameters, the coating fluid properties, and the

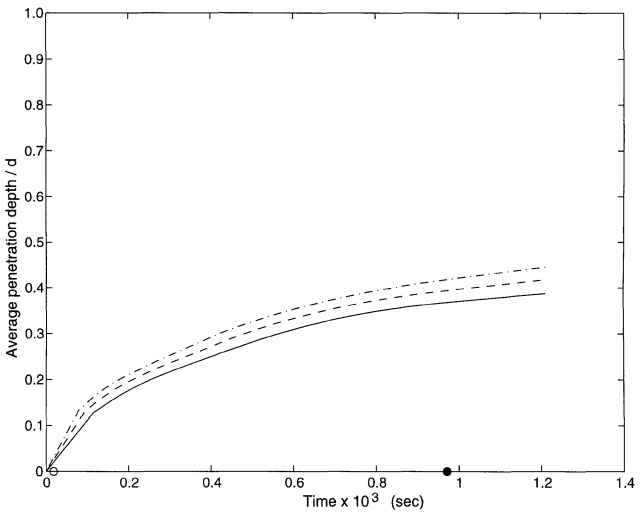

Figure 17. Effect of the surface tension σ.

The results are, from bottom to top, for $\sigma = 30$, 40 and 50 cp. The coating fluid's viscosity is $\eta = 5$ cp.

boundary conditions, on fluid imbibition into paper during coating operations. In general, based on the simulation results, the viscosity and surface tension of the coating fluid are its most important properties in terms of their effect on the fluid imbibition. The convective pressure distribution, applied to the top surface of the paper, as well as the web speed, are also important parameters. These parameters can, of course, be manipulated or adjusted easily. The microstructural characteristics of the paper, on the other hand, though very important, can be adjusted only by changing the paper type used in the coating operation, which points to the significance of characterization of its pore space.

In future papers we will report the results of a novel method of characterizing the microstructure of papers, which will then be used in the simulator developed in this article. We will also utilize a non-Newtonian fluid model for representing the

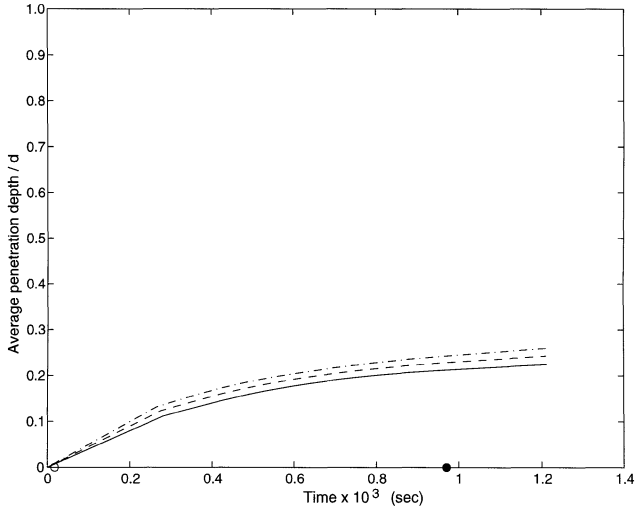

Figure 18. Same as in Figure 17, but for a coating fluid viscosity of $\eta = 20$ cp.

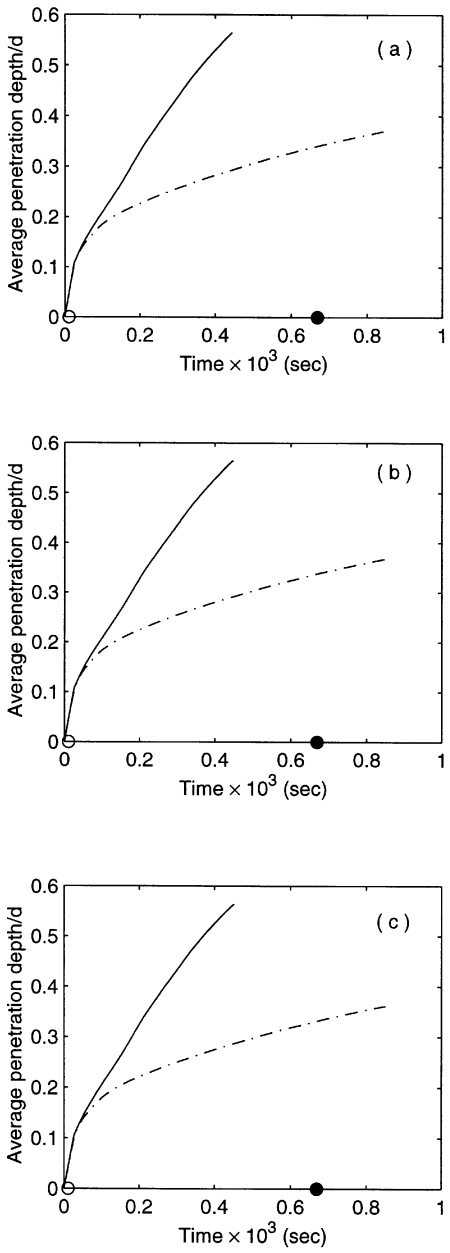

Figure 19. Comparison of the average penetration depths resulting from applying a convection-driven pressure (solid curves) and an atmospheric pressure (dashed curves).

The results are for contact angles $\theta = 10°$, 20° and 30°, respectively.

coating fluid, and utilize the dynamic contact angle in our simulations. These improvements will enable us to make a quantitative comparison between the simulator's predictions and experimental data.

Acknowledgments

This work was initiated while M.S. was spending his sabbatical leave at Avery Dennison Research Center, and was continued when J.G. spent the Summer of 1998 at the Center. They both thank Avery Dennison Corporation for financial support and the staff of the Center for their warm hospitality and stimulating discussions. The continuation of this work at USC was also supported by Avery Dennison Corp., as well as in part by the Petroleum Research Fund, administered by the American Chemical Society.

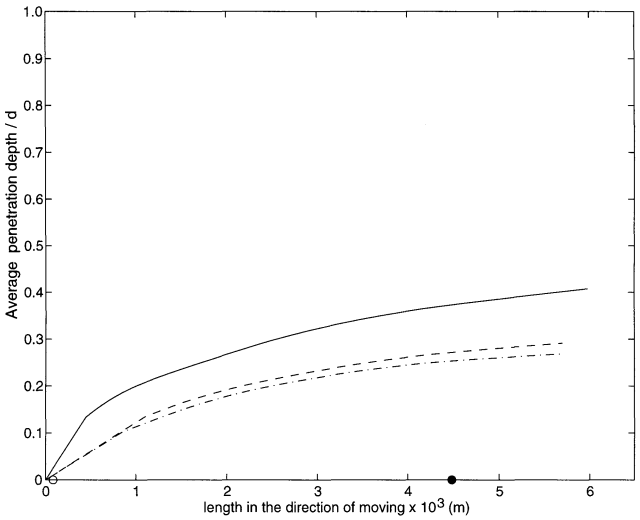

Figure 20. Effect of the convection-driven pressure distribution applied at the paper's top surface for, from top to bottom, Cases 1, 2 and 3 (see Table 1).

Literature Cited

Blunt, M. J., and H. Scher, "Pore-Level Modeling of Wetting," *Phys. Rev. E*, **52**, 6387 (1995).

Chen, K. S. A., and L. E. Scriven, "Liquid Penetration into Deformation Porous Substrate," *Tappi J.*, **73**, 151 (1990).

Cieplak, M., and M. O. Robbins, "Influence of Contact Angle on Quasistatic Fluid Invasion of Porous Media," *Phys. Rev. B*, **41**, 11508 (1990).

Cox, R. G., "The Dynamics of the Spreading Liquids on a Solid Surface. Part 1. Viscous Flow," *J. Fluid Mech.*, **168**, 169 (1986).

Danino, D., and A. Marmur, "Radial Capillary Penetration into Paper: Limited and Unlimited Liquid Reservoirs," *J. Colloid Interface Sci.*, **166**, 245 (1994).

de Gennes, P. G., "Dynamic Capillary Pressure in Porous Media," *Europhys. Lett.*, **5**, 689 (1988).

Deng, M., and C. T. J. Dodson, *Paper: An Engineered Stochastic Structure*, Tappi Press, Atlanta (1994).

Dodson, C. T. J., and W. K. Ng, "Paper Stochastic Structure Analysis," Pulp & Paper Center, University of Toronto preprint (1994).

Dodson, C. T. J., and W. W. Sampson, "The Effect of Paper Formation and Grammage on its Pore Size Distribution," Pulp & Paper Center, University of Toronto preprint (1995).

Dullien, F. A. L., *Porous Media: Fluid Transport and Pore Structure*, 2nd ed., Academic Press, New York (1992).

Hashemi, M., B. Dabir, and M. Sahimi, "Dynamics of Two-Phase Flow in Porous Media: Simultaneous Invasion of Two Fluids," *AIChE J.*, **45**, 1365 (1999).

Haynes, R. E., F. H. Bertrand, and P. A. Tanguy, "Modelling of Fluid/Paper Interaction in the Application Nip of a Film Coater," *Transport in Porous Media*, **40**, 55 (2000).

Hellén, E. K. O., M. J. Alava, and K. J. Niskanen, "Porous Structure of Thick Fiber Webs," *J. Appl. Phys.*, **81**, 6425 (1997).

Jerauld, G. R., L. E. Scriven, and H. T. Davis, "Percolation and Conduction on the 3D Voronoi and Regular Networks: A Second Case Study in Topological Disorder," *J. Phys. C*, **17**, 3429 (1984).

Koponen, A., D. Kandhai, E. Hellen, M. Alava, A. Hoekstra, M. Kataja, K. Niskanen, P. Sloot, and J. Timonen, "Permeability of Three-Dimensional Random Fiber Webs," *Phys. Rev. Letts.*, **80**, 716 (1998).

Lyne, M. B., and J. S. Aspler, "Wetting and the Sorption of Water by Paper under Dynamic Conditions," *Tappi J.*, **67**, 98 (1982).

Mathews, T., G. P. Matthews, C. J. Ridgway, and A. K. Moss, "Measurement of Void Size Correlation in Inhomogenous Porous Media," *Transport in Porous Media*, **28**, 135 (1997).

Matthews, G. P., C. J. Ridgway, and M. C. Spearing, "Void Space Modeling of Mercury Intrusion Hysteresis in Sandstone, Paper Coating, and other Porous Media," *J. Colloid Interface Sci.*, **171**, 8 (1995).

Oliver, J. F., "Wetting and Penetration of Paper Surfaces," in *Reprographic Technology*, American Chemical Society, Washington, DC, p. 435 (1982).

Oliver, J. F., L. Agbezuge, and K. Woodcock, "Development of a Realistic Drying Model for Water-based Ink Jets Inks Printed on Paper," *Proc. IS & T's Intl. Cong. on Advances in Non-impact Printing Technol.*, Portland, OR, p. 163 (1991).

Pan, S. X., H. T. Davis, and L. E. Scriven, "Modeling Moisture Distribution and Binder Migration in Drying Paper Coatings," *Tappi J.*, **78**(8), 127 (1995).

Poulin, N., P. A. Tanguy, J. Aspler, and L. Larrondo, "Numerical and Physical Modeling of the Permeability of Paper to CMC and Coating Liquids," *Can. J. Chem. Eng.*, **75**, 949 (1997).

Qi, D., and T. Uesaka, "Numerical Experiments on Paper-Fluid Interaction—Permeability of a Three-Dimensional Anisotropic Fiber Network," *J. Mater. Sci.*, **31**, 4865 (1996).

Räisänen, V. I., M. J. Alava, and R. M. Nieminen, "Failure of Planar Fiber Networks," *J. Appl. Phys.*, **82**, 3747 (1997).

Rothman, D. H., and S. Zaleski, *Lattice-Gas Cellular Automata*, Cambridge University Press, Cambridge (1997).

Sahimi, M., "Flow Phenomena in Rocks: From Continuum Models to Fractals, Percolation, Cellular Automata and Simulated Annealing," *Rev. Mod. Phys.*, **65**, 1393 (1993).

Sahimi, M., *Flow and Transport in Porous Media and Fractured Rock*, VCH, Weinheim, Germany (1995).

Sartor, L., "Slot Coating: Fluid Dynamics and Die Design," PhD Thesis, Univ. of Minnesota (1990).

Scharcanski, J., and C. T. J. Dodson, "Texture Image Analysis for Paper Anisotropy and its Variability," Pulp & Paper Center, University of Toronto Preprint (1995).

Selim, M. S., V. F. Yesavage, R. Chebbi, H. S. Sung, J. Borch, and J. M. Olson, "Drying of Water-Based Inks on Plain Paper," *J. Imag. Sci. Technol.*, **41**, 152 (1997).

Stokes, J. P., M. J. Higgins, A. P. Kushnik, S. Bhattacharya, and M. O. Robins, "Harmonic Generation as a Probe of Dissipation at a Moving Contact Line," *Phys. Rev. Lett.*, **65**, 1885 (1990).

Manuscript received Mar. 27, 2000, and revision received Aug. 28, 2000.